Linear contracting and air-stable electrochemical artificial muscles based on commercially available CNT yarns and ionically selective ionogel coatings

Bin Ni, Frédéric Braz Ribeiro, Cédric Vancaeyzeele, Giao T.M. Nguyen, Edwin W.H. Jager, Cédric Plesse, Frédéric Vidal

Applied Materials Today 31 (2023) 101756

Contents lists available at ScienceDirect

Applied Materials Today

journal homepage: www.elsevier.com/locate/apmt

Linear contracting and air-stable electrochemical artificial muscles based on commercially available CNT yarns and ionically selective ionogel coatings

Bin Ni [a], Frédéric Braz Ribeiro [a], Cédric Vancaeyzeele [a], Giao T.M. Nguyen [a], Edwin W.H. Jager [b], Frédéric Vidal [a], Cédric Plesse [*,a]

[a] Laboratoire de Physicochimie des Polymères et des Interfaces, Institut des Matériaux, CY Cergy Paris Université, 95000 Neuville sur Oise, France
[b] Division of Sensor and Actuator Systems Department of Physics, Chemistry, and Biology (IFM)Linköping UniversityLinköping SE-581 83, Sweden

ARTICLE INFO

Keywords:
Artificial muscle
Poly (ionic liquid)
Coiled CNT
Ionoelastomer
Linear contractile stroke

ABSTRACT

Artificial muscles, or soft actuators, that could exhibit contractile stroke and operate in open-air, would be crucial for many applications, such as robotics, prosthetics, or powered exoskeletons. Amongst the different artificial muscle technologies, electrochemical carbon nanotube (CNT) yarn muscles, transducing capacitively ionic accumulation at the electrochemical double layer into linear contraction, are amongst the most promising candidates. However, their performances are either limited by an undesired bipolar behaviour or short lifetime due to the inevitable drying of water-based electrolytes. In this paper, we present here the fabrication of air-operating contractile linear artificial muscles from commercially available CNT yarns exhibiting outstanding performance. The synthesis and the junction of two ionogels based on cationic and anionic polyelectrolyte have been designed for the coating process on CNT yarns, and for selectively orienting the ionic flow allowing optimal electromechanical energy conversion. The dual-electrode CNT yarn actuators showed air-stable unipolar contractile stroke, reaching 9.7% without loss of performances after 2000 cycles.

1. Introduction

Artificial muscles, i.e. soft actuators that mimic the behaviour and features of biological muscles, have attracted much interest due to their various applications in robotics [1], prosthetics [2], or powered exoskeletons [3]. Many types of artificial muscle materials have been extensively studied, such as thermal-driven muscles [4,5], pneumatic-driven muscles, and [6,7] electrochemically driven muscles [8,9]. amongst the numerous available stimuli-responsive materials, electro-chemically-driven devices stand out because of their low operating potential, higher energy conversion efficiency and better controllability [10].

As electrochemically driven muscle, carbon nanotube (CNT) yarns are especially promising because of the advantages of high strength and high electrical conductivity [11–14]. Their working principal relies on the charging/discharging of the electrochemical double layer (EDL) at the CNT-electrolyte interface through capacitive process, transducing a low-voltage electrochemical stimulation into electrode's volume variation thus into mechanical response. Interestingly, when the neat CNT yarns are coiled by overtwisting, they can convert torsional actuation into contractile deformation upon electrochemical stimulation, reaching ~ 4% of deformation in aqueous electrolyte [13] and up to 16.5% in organic electrolyte [12]. Indeed, upon charging the EDL Capacitor (EDLC), the ion's influx into electrodes promotes a local increase in volume and consequently an overtwisting of the coil, expanding in diameter and contracting in length. During the EDLC discharge, the ion's efflux is promoting the opposite phenomenon and leads to an elongation of the coiled yarns. By associating two coiled CNT yarns, acting as electrodes of an EDLC and by using a gel electrolyte, it becomes possible to achieve open-air linear actuation [12]. However, the symmetric nature of these open-air devices enables the charging of the EDLC indifferently under positive or negative potential bias due to anions or cations influx. Consequently, this so-called bipolar behaviour promotes a contraction of the coiled CNT yarns during any electrical stimulation and the net contractile stroke is *de facto* limited by the difference between the discharged/elongated state at 0 V and the charged/contracted state under either positive or negative tension. Nevertheless, this bipolar behaviour can be circumvented by selectively allowing one type of ion

* Corresponding author.
E-mail address: cedric.plesse@cyu.fr (C. Plesse).

https://doi.org/10.1016/j.apmt.2023.101756
Received 21 July 2022; Received in revised form 24 December 2022; Accepted 29 January 2023
Available online 10 February 2023

to charge the EDLC and selectively blocking the other one during reversed potential bias. This unipolar behaviour has been recently achieved by Baughman and coworkers thanks to the coating of CNT yarns with water based cationic or anionic polyelectrolytes as ion selective layers [11]. The deformation of individual coiled yarns could occur unidirectionally across the full potential window and is consequently maximized. When combining two CNT yarns coated respectively with cationic and anionic polyelectrolyte and an aqueous based electrolyte, open-air unipolar CNT yarn muscles were obtained with a 3.9% stroke and integrated into actuating textiles [11].

However, this family of artificial muscles has a limited operational lifetime in open-air, due to the inevitable drying issues of aqueous or volatile organic electrolytes, which results in a rapid drop of the performance. This demonstrated the need for in air-stable ionic sources [15–18].

For that purpose, ionogels, i.e. polymer networks percolated with non-volatile ionic liquids (ILs), are especially interesting since they are ionic sources that combine solvent-free high ionic conductivity, suitable mechanical properties, and air stability [19–22]. The association of ILs with anionic or cationic polyelectrolytes, acting as ion-selective layers, appears as a very promising approach to develop unipolar CNT yarn muscles with in air-stable ionic sources.

Here, we describe the development of an original unipolar CNT artificial muscle that exhibits an outstanding contractile stroke of 9.7% upon low voltage stimulation and is able to have a long operational time in the open-air. It is achieved by (i) developing ionically selective coating based on polymeric ionic liquid (PIL) ionogels by using either polycationic or polyanionic PIL, (ii) their coating on commercially available CNT yarns that are coiled to enhance their electromechanical deformation and (iii) the creation of a cationic-anionic junction between the two coated yarns, similar to that recently described for ionotronics [23]. The polycationic ionogel coated on a first coiled CNT electrode will permit the anodic charging/contraction thanks to anion's influx but will also block the cathodic charging of this electrode under reversed bias by acting as an ion selective layer hindering cation's influx. Similarly, the polyanionic ionogel coated on the second coiled CNT electrode will permit the cathodic charging/contraction of this electrode by cation influx and will block its anodic charging by hindering anion's influx (Fig. 1a). Thus, the two yarns can actuate in a cooperative manner upon applying a voltage, both contracting during application of a positive bias between the polycationic and polyanionic coating yarns and both elongating during the reverse bias, leading to the so-called unipolar behaviour.

In this work, the ionic liquid was first selected and their analogue polyanionic and polycationic PILs were designed and synthesized. The polycationic and polyanionic ionogels were synthesized using semi-

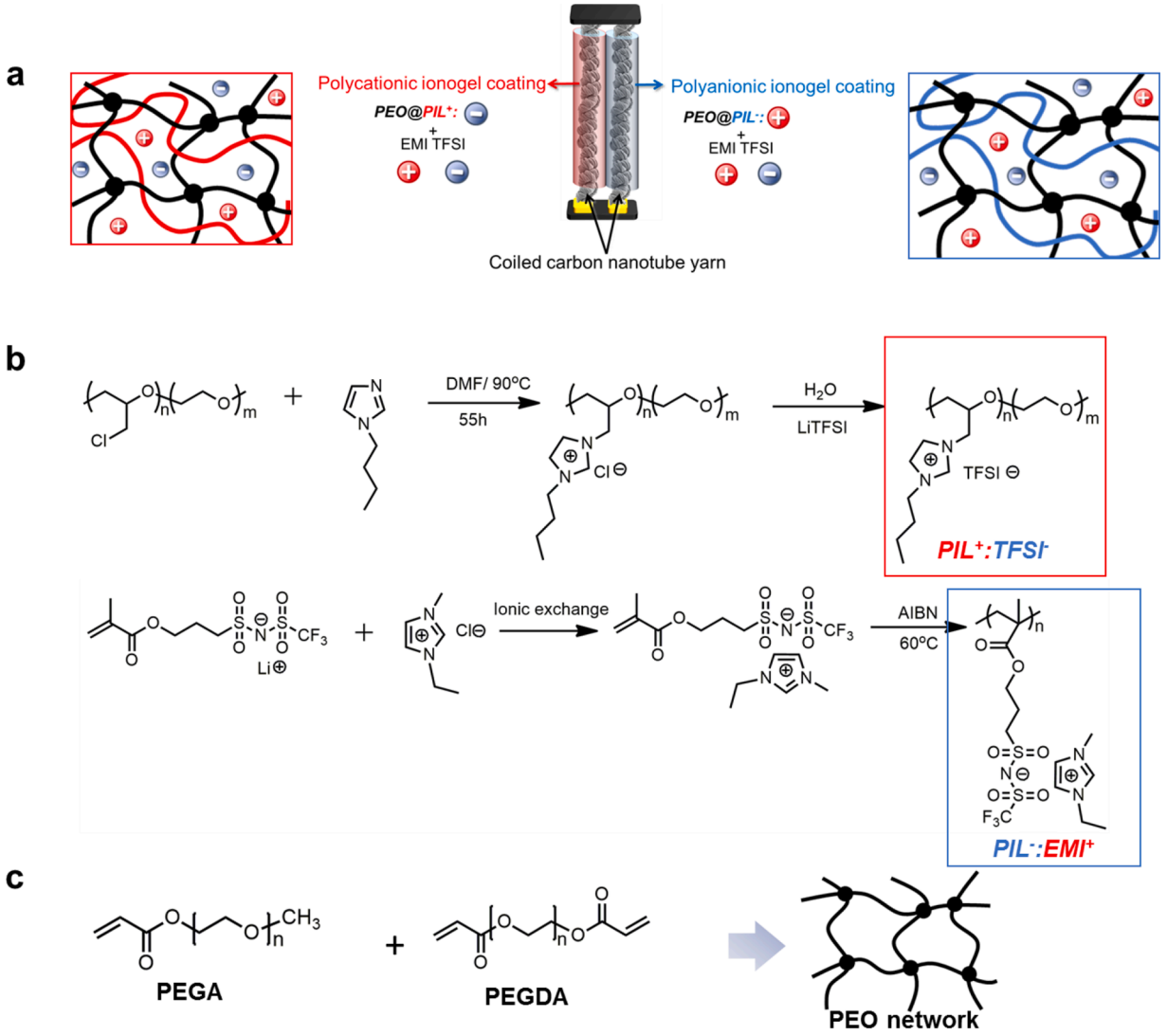

Fig. 1. (a) Scheme of the open-air CNT artificial muscles based on the junction of polycation and polyanionc ionogel coatings. (b) The synthetic route of PIL^+:$TFSI^-$ and PIL^-:EMI^+. (c) scheme of the PEO network formation.

interpenetrating polymer network architecture where the PIL is entangled in a polymer network obtained from UV free radical polymerization of polyethylene oxide (PEO) acrylate precursors. The two PIL ionogel coatings have been optimized (i) to be endowed identical ionic conductivity, despite their opposite mobile ionic species, and (ii) to present a low initial viscosity and fast curing time making them suitable for homogeneous coatings on yarns. While the polycationic and polyanionic nature of the coating is transitioning the CNT artificial muscles from bipolar to unipolar stroke, the ionic liquid-based gel ensures electrochemical stability and the long life open-air operation. Moreover, the response speed of the dual-electrode actuator was significantly enhanced by either decreasing the interval distance between two electrodes or applying higher potential with short pulse times. To our best of knowledge, this is the first time PILs have been found to enable the unipolar stroke behaviour while intrinsically allowing the development of solid state and open-air-stable electrochemical CNT muscles. These dual-electrode actuators are ideal candidates to be deployed in electromechanically active textiles as textile muscles or haptic textiles [24–27].

2. Materials and methods

2.1. Materials

Poly(ethylene glycol) diacrylate (PEGDA, Mn = 700 g mol^{-1}, Aldrich), poly(ethylene glycol) methyl ether acrylate (PEGA, Mn = 480 g mol^{-1}, Aldrich), 2-Hydroxy-2-methylpropiophenone (97%, Sigma-aldrich), Carbon nanotube yarns (DexMat, Galvorn CNT yarns, diameter = 150 μm; resistance = 10 Ω/m), poly(epichlorohydrin-co-ethylene oxide) (Hydrin® C2000XL, m:*n* = 1:1, Mw = 8.73×10^6 g/mol, Mw/Mn = 4.5), 1-Butylimidazole (98%, alfa-acesar), lithium bis(trifluoromethylsulfonyl)imide (LiTFSI, 99%, Solvionic), Lithium sulfonyl (trifluoromethane sulfonyl)imide methacrylate (MTFSI:Li, Specific polymer), 1-methyl-3-ethylimidazolium chloride (TCI, 98%), 1-ethyl-3-methylimidazolium bis-(trifluoromethanesulfonyl)imide (EMITFSI, Solvionic, electrochemical grade 99%), N,N-dimethylformamide (DMF, anhydrous 99,8%, Acros), pentanone and acetone (VWR, AR), 2,2′-Azobis(2-methylpropionitrile) (AIBN, Aldrich, initiator) was recrystallized from ethanol before using.

2.2. Methods

2.2.1. NMR characterization

^{1}H NMR spectra were recorded on a Bruker AVANCE 400 MHz spectrometer at 297 K. Deuterated chloroform ($CDCl_3$) and Deuterated acetone (C_3D_6O) were used as the solvent.

Mechanical properties: Tensile experiments were conducted on a Dynamic Mechanical analyzer instrument (TA, Q800) in tensile mode at 30 °C with strain rate of 100%·min^{-1} to 500%. An initial strain of 0.05% and a preload force of 0.01 N was performed to obtain stress-strain curves.

2.2.2. Polymerization speed characterization

Photopolymerization speed was recorded by rheometer. Rheological measurements were performed with an Anton Paar Physica MCR 301 rheometer equipped with CTD 450 temperature control device and a plate−plate geometry (Gap 250 μm, diameter 25 mm, plate: polymerization system made from a lower glass plate coupled with UV Source Omnicure 154 mW/cm^2). A 1% deformation was imposed at 1 Hz. Storage modulus (G') and loss modulus (G") were recorded as a function of time. The solution of precursors of materials was put in the rheometer geometry at 30 °C and measurements began immediately, and UV exposure is delayed in time.

2.2.3. Ionic conductivity

The ionic conductivity was recorded by electrochemical impedance spectroscopy using a VSP 150 potentiostat (biologic SA). Samples were first dried under vacuum 60 °C for 1 day before characterization. Experiments were carried out at room temperature in the frequency range from 2 MHz to 1 Hz with a rate of 6 points per decade and at 0 V with an oscillation potential of 10 mV. The ionic conductivity (S·cm^{-1}) is calculated using $\sigma = h/(Z^*S)$, where Z is the real part of the complex impedance (ohms), h is the thickness of the sample (cm), and S is the sample area (cm^2).

2.2.4. Scanning electron microscopy (sem)

SEM was performed using a Carl Zeiss AG-ULTRA 55 by GEMINI with a field emission gun at 2–10 kV.

2.2.5. Electrochemical characterization

Capacitance was calculated by cyclic voltammetry (CV) tests, which were performed by cycling the potential between 1 V and –1 V for the dual-electrode actuator with solid electrolyte at different scan rates. The working electrode was connected to coiled CNT coated with polycationic ionogel. And the counter electrode was linked with coiled CNT coated with polyanionic ionogel.

2.2.6. Stroke deformation characterization

The length of the actuator was kept by connecting them with an isometrically operated force-displacement lever arm transducer (Aurora Scientific model 300C, Canada) with 25 mN preloading.

2.2.7. Energy density determination

The actuator was kept by connecting them with an isometrically operated force-displacement lever arm transducer (Aurora Scientific model 300C, Canada) with 25 mN, 50 mN, 75 mN, 100 mN and 1.25 N preloading, respectively. The move distance of the actuator at different preloading were recorded. The energy density was calculated as (F*d)/w, where F is the force (N), d is the moved distance (m), and w represents the actuator total weight (kg).

2.2.8. Synthesis of PIL^+:$TFSI^-$

4 g of C2000XL is solubilized in 23 mL DMF for 3 h at 80 °C under reflux. 10 equivalents of the distilled 1-butylimidazole (36.33 g) is added to the solution once the polymer has been solubilized. The reaction takes 55 h at 90 °C under reflux and results in a colourful solution. The reaction medium is then reprecipitated in acetone (1:5 vol.). After that, the reaction medium is reconstituted in acetone (1:5 vol.). The polymer is washed with a lot of acetone and then dried under dynamic vacuum for 2 h at 30 °C. This intermediate is solubilized in a minimum amount of distilled water. 2.2 equivalents of LiTFSI salt are dissolved in water at the same time. (1:2.5 wt.). Finally, the PIL intermediate solution is added drop by drop to the LiTFSI solution and the ion-exchange from Cl^- to $TFSI^-$ takes place. The obtained polymer (PIL^+:$TFSI^-$) is washed with distillated water and dried at least one week under dynamic vacuum at 70 °C. ^{1}H NMR spectrum of the polymer is shown in the Figure S1a.

2.2.9. Synthesis of PIL^-:EMI^+

The monomer ($MTFSI^-$:EMI^+) is synthesized through an ion exchange reaction between the Li^+ ion and the cationic imidazolium. 0.1% inhibitor was added to avoid the rapid oligomerization of MTFSI. The 1-methyl-3-ethylimidazolium chloride (0.94 g), Lithium sulfonyl (trifluoromethane sulfonyl)imide methacrylate (0.4 g), water (2 mL) and 1.34 mg inhibitor were added into one flask. The mixed solution reacted at RT for 24 h with continuous magnetic stirring. After the reaction, Dichloromethane as the solvent to extract the monomer from the solution. Finally, a rotary evaporator was used to remove the solvent and then dynaymic vacumm for one day at room temperature to obtain the yellow liquid. Yield (94%). (^{1}H NMR – Figure S1b: -N-C*H*═N-, 9.2 ppm; -N-C*H*—CH—N-, 7.20 ppm; -N-CH—C*H*—N-, 7.19 ppm; -CH_2═C-, 6.02 ppm, 5.56 ppm;-O-CH_2–CH_2-, 4.3 ppm; -N-CH_2–CH_3; -N-CH_3, 3.95

ppm;-CH_2-S-, 3.35 ppm; -CH$_2$–CH_2–CH$_2$-, 2.20 ppm; CH$_2$=C—CH_3, 1.85 ppm; -N-CH_2–CH_3, 1.49 ppm). The MTFSI$^-$:EMI$^+$monomer was then polymerized. 0.6 g MTFSI$^-$:EMI$^+$, 0.3 g DMF, and 6 mg AIBN were added into a tube enclosed by a rubber cover. Two-needle were inserted into the rubber cover, one was connected to the vacuum pump and another was associated with argon balloon. First, liquid N_2 was used to freeze the mixed solution, avoiding solvent evaporation during the vacuum process. Then, vacuuming for 10 min via gas pump to remove the gas inside the tube and then thaw the frozen solution with Argon gas. The frozen and thaw processes were performed three times to remove the residual O_2 from the solution. Finally, the tube with argon gas inside was immersed into an oil bath (60 °C) to polymerize for 20 h. The gel phenomenon would be observed after polymerization. Using a small amount of acetone (~1:1 to the obtained gel) to dilute the synthesized polymer gel and then precipitate it in a large amount of ethyl acetate. The white flocculent precipitation could be obtained. A dynamic vacuum was finally used to remove the solvent. The dry PIL$^-$:EMI$^+$ was obtained. ^{1}H NMR spectrum of the polymer is shown in the Figure S1c. Yield (80%).

2.2.10. s-IPN PEO@PILs films preparation

PEG mixture including PEGA and PEGDA, PILs (PIL:EMI or PIL:TFSI), solvent(Acetone or Pentanone), and photoinitiator (Hydroxy-2-methylpropiophenone) were added into the glass bottle with the formulations in Table 1. They were then mixed for 20 s to obtain the homogeneous solution using a vortex mixer. The mixed solution was then drop-casted onto a glass surface with a PTFE mould of which the thickness is 500 μm. Finally, the photopolymerization was performed by UV bench (100 W/cm^2) for 10 times (6 s/time). Dymanic vacumm was carried out to remove the solvent at 60 °C for one day, Finally, the s-IPN films were obtained.

2.2.11. s-IPN PEO@PILS@EMITFSI ionogel preparation

PEG mixture composed of 75% PEGA and 25% PEGDA, PILs (PIL:EMI or PIL:TFSI vs PEG mixture = 40 wt%: 60 wt%), solvent (acetone vs PIL:EMI = 1:2.5 or pentanone vs PIL:TFSI = 1:2), EMITFSI (50 wt% to the final ionogel) and photoinitiator (Hydroxy-2-methylpropiophenone, 2wt% vs PEG mixture) were added into the glass bottle with homogeneous mixing. The mixed solution was drop-casted onto a glass surface with a PTFE mould of which the thickness is 500 μm. Finally, the photopolymerization was performed by UV bench (100 W/cm^2) for 40 times (6 s/time), Dymanic vacumm was carried out to remove the solvent at 60 °C for one day. The “dry” film was obtained.

2.2.12. The fabrication of dual-electrode actuators

The linear CNT was coiled by a home-made designed device. The process was shown in Scheme S1. Before the coiling technique, ozone treatment was conducted for 1 min on the CNT surface to enhance the wettability with ionic precursors. The PEO@PIL$^-$:EMI$^+$@EMITFSI ionogel precursors was dropped onto the treated CNT, and then the CNT was clockwise twisted with constant 5 MPa preloading until to the completely coiled state. The length of CNT was changed from 4.1 cm to 0.9 cm. Finally, UV lamp (154 mW/cm^2) was used to initiate the polymerization for 5 mins. One electrode with solid electrolyte was obtained.

Table 1
Formulation of the s-IPN network with different contents of PEO and PILs.

Sample	PEG mixture (molar ratio)		PEG mixture: PIL (weight ratio)	PIL: Solvent (weight ratio)	
	PEGA	PEGDA			
1	75%	25%	50:50	PIL$^+$:TFSI$^-$: Pentanone (1: 2)	PIL$^-$:EMI$^+$: Acetone (1: 2.5)
2			60:40		
3			70:30		
4			80:20		

The same procedure was conducted to prepare another electrode with The PEO@PIL$^+$:TFSI$^-$@EMITFSI ionogel precursors. Finally, the dual-electrode actuator was fabricated by gluing two electrodes together. The PEO@PIL$^-$:EMI$^+$@EMITFSI ionogel precursors mixture was always acted as the glue. It was worth noting that coating processes were performed three times for each electrode during the preparation of dual-electrode actuator with 1 mm interval distance. Only one coating for each electrode to prepare the actuator with interval distance of 0.45 mm.

3. Results and discussions

The strategy to develop in open-air-operating CNT muscles with linear unipolar stroke relies on fabricating a coiled CNT dual-electrode device with respectively polyanionic and polycationic ionogel coatings (Fig. 1a).

3.1. Development of ionically selective coating based on pil ionogels

First, 1-ethyl-3-methylimidazolium (EMI$^+$) and bis(trifluoromethylsulfonyl)imide (TFSI$^-$) were selected as cations and anions of the IL because of their similar ionic radius [28,29], which could allow symmetric electromechanical deformation on the two electrodes, as well as for their good ionic dissociation and excellent ionic conductivity [30]. PILs are defined as a subclass of polyelectrolyte containing ionic liquid like ions grafted on their backbone. In our case, two PILs containing TFSI$^-$ and EMI$^+$ were considered: polycationic with TFSI$^-$ as mobile counter-ion (PIL$^+$:TFSI$^-$) and polyanionic with EMI$^+$ mobile counter-ions (PIL$^-$:EMI$^+$) (Fig. 1b). The polycationic PIL (PIL$^+$:TFSI$^-$) was synthesized from commercially available poly (epichlorohydrin-co-ethylene oxide) copolymer by introducing imidazolium pending groups to the polymer backbone, using TFSI$^-$ as counter ions according to the previously described method (Fig. 1b) [31]. The polyanionic PIL (PIL$^-$:EMI$^+$) was obtained by polymerization of TFSI$^-$ bearing methacrylate with EMI$^+$ as counter ions, that can be obtained by simple ionic exchange of commercially available lithium sulfonyl(trifluoromethane sulfonyl)imide methacrylate (MTFSI:Li) precursor (Fig. 1b). The synthesis and characterisation of PILs are detailed in Supplementary Information. Semi-interpenetrating polymer networks (s-IPNs) based on PEO acrylate network as shown in the Fig. 1c and entangled polycationic (PIL$^+$:TFSI$^-$) or polyanionic (PIL$^-$:EMI$^+$) linear polymers were synthesized as the polymer component of the ionogels, as schematized in the Fig. 1a.

The preparation of the PIL based coatings relies on mixing the desired amount of PIL with the acrylate precursors of the PEO network, i.e. poly(ethyleneglycol)acrylate (PEGA) and poly(ethyleneglycol)diacrylate (PEGDA) and follows by a free-radical photopolymerization of the later. The detailed composition of the reactive mixtures is reported in Table S1. Precursors mixtures of both PIL ionogel have a low viscosity of less than 1 Pa·s, making them appropriate for coating. Their rheological behaviour upon UV-irradiation (Fig. 2a and 2b) indicated their rapid gelation time (< 20 s) that allows a fast and homogeneous coating of the CNT yarns. The mechanical properties s-IPN free-standing films at different PEO:PIL weight ratio (Fig. 2c and 2d) as well as their ionic conductivity (Fig. 2e and 2f) were then characterized. In general, increasing PIL content increases the material strain and decreases their Young’s modulus. The presence of PEO in the s-IPN allows improving the ionic transport in the material, thus improving the ionic conductivity. As a result, the s-IPNs with a 60:40 wt ratio of PEO network to PIL were identified as the best candidate for the ionogel host matrix, with a low Young modulus < 1 MPa, an elongation at break up to 90%, and a liquid-free ionic conductivity already above 10^{-5} S/cm. These PIL s-IPN will be named as PEO@PIL$^+$:TFSI$^-$ or PEO@PIL$^-$:EMI$^+$.

The corresponding polycationic and polyanionic ionogels, made of PEO@PILs in 60:40 wt proportions were finally synthesized in the presence of EMITFSI (50 wt% vs. materials weight) and are named

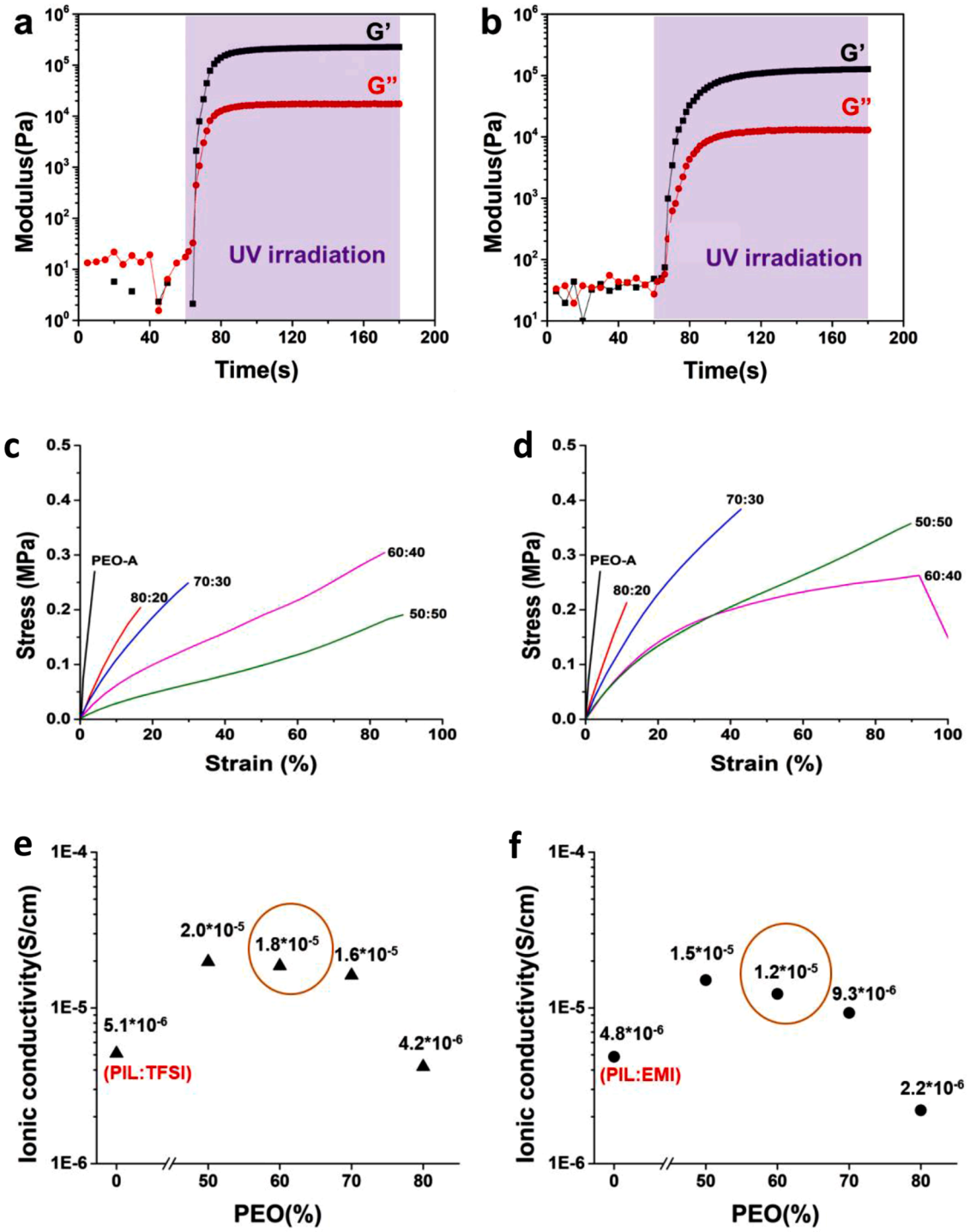

Fig. 2. Polymerization kinetics of s-IPN formation followed by rheometer. Precursor solution contains PEG mixture and different PILs (60/40 wt ratio). (a) PIL^+:$TFSI^-$, (b) PIL^-:EMI^+. The mechanical properties of s-IPN films at different weight ratios between PEO and PILs, assigned as [PEO]:[PIL]. (c) PIL^+:$TFSI^-$; (d) PIL^-:EMI^+. The ionic conductivity of s-IPN films as a function of PEO network weight ratios. (e) PIL^+:$TFSI^-$; (f) PIL^-:EMI^+.

PEO@PIL^+:$TFSI^-$@IL and PEO@PIL^-:EMI^+@IL, respectively. The presence of EMITFSI in PEO@PIL material results in ionogels with increased ionic conductivity reaching ~5 × 10^{-3} S/cm (4.5 × 10^{-3} S/cm for PEO@PIL^+:$TFSI^-$@IL and 5.8 *10^{-3} S/cm for PEO@PIL^-:EMI^+@IL), which was ~ 300 times higher than that of the initial s-IPN.

3.2. Dual-electrode actuator fabrication

In this study, we have selected ready-to-use commercially available CNT yarns allowing bypassing lab-scale complex and optimized production [11]. The coiling of the chosen yarns is performed under 5 MPa constant preload with around 50 turns/cm. The morphologies of the commercial yarns and of the corresponding coiled CNT are shown in Fig. 3a and 3b, respectively. The commercial CNT is composed of three bundles of CNT fibers. After coiling, the CNT exhibited a loose and relatively open surface appearance, contrary to the tightness of coiled custom-made CNT yarns reported in literature [11,12,32]. The detailed coating process and actuator fabrication are shown in Fig. 3c. For in

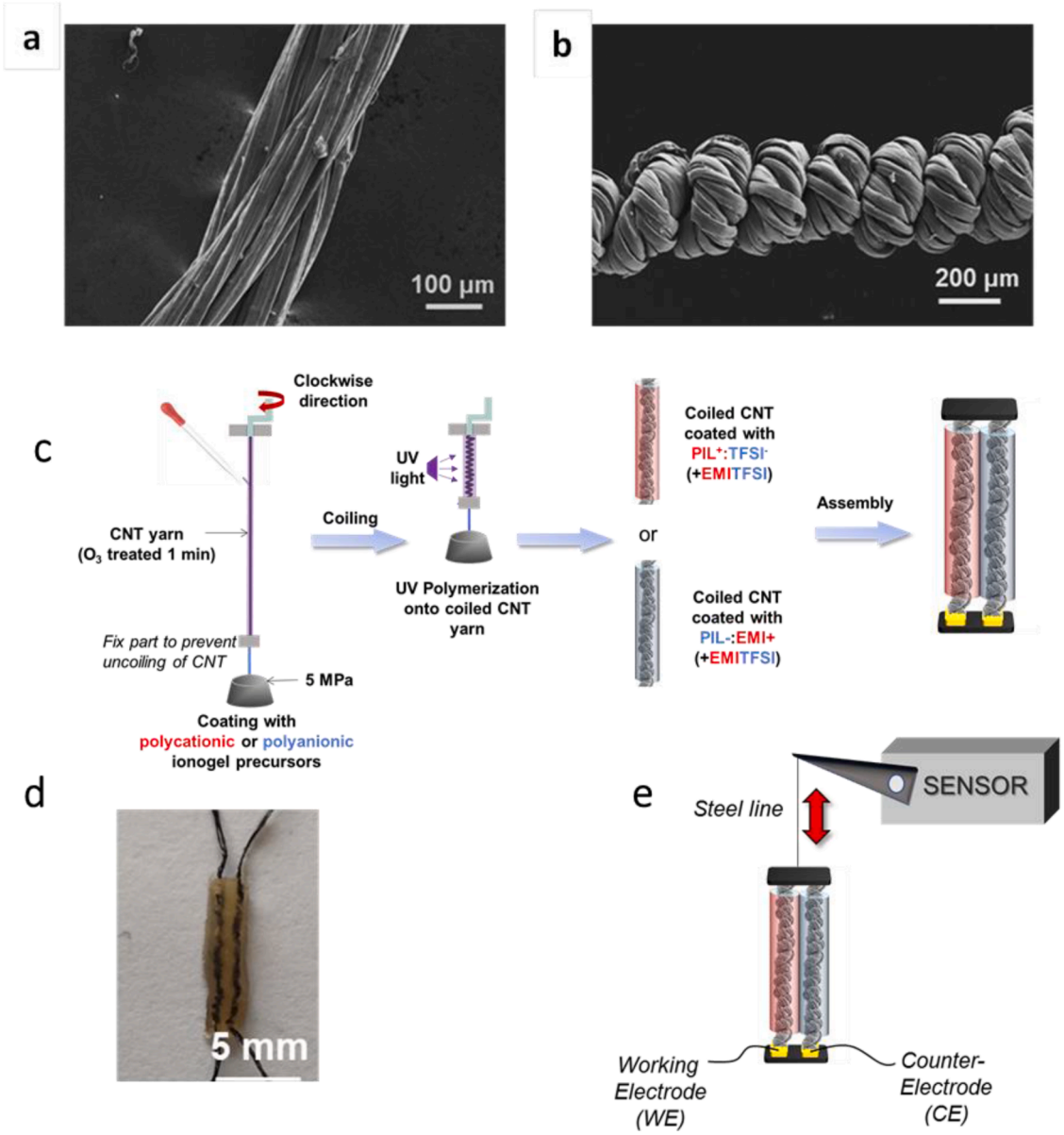

Fig. 3. SEM images of (a) as-received linear CNT and (b) coiled CNT, (c) Schematic illustration of coiling process of CNT and the preparation of dual-electrode actuator. (d) Photo of a dual-electrode actuator with a 1mm-gap between the two coiled CNT yarns. (e) The schematic illustration of stroke and force characterization for the dual-electrodes actuator.

open-air actuation, two coiled CNT yarns are used as the actuator electrodes. First, CNT yarn was surface-treated with O_3 and then coated with polycationic PEO@PIL$^+$:TFSI$^-$ precursors or with those of polyanionic PEO@PIL$^-$:EMI$^+$, with or without EMITFSI. The two pre-coated CNT yarns were coiled separately. After UV-exposition to trigger the photopolymerization of the precursors, the two yarns were assembled together using an extra layer of PEO@PIL$^-$:EMI$^+$ precursors acting as UV-curable ionically conducting glue [33]. The resulting dual-electrode actuator was obtained with an interval of ~1 mm between the two electrodes (Fig. 3d). Actuator based on PEO@PIL was fabricated for using as reference and named PEO@PIL actuators, and those fabricated in the presence of EMITFSI named PEO@PIL@IL actuators.

3.3. Actuation performance of dual-electrode actuator

Dual electrode actuators were studied using the electromechanical setup presented in the Fig. 3e. First, the actuators have been characterized by cyclic voltammetry −1 V to 1 V at difference scan rate and the capacitance was presented as a function of scan rate (Figure S2). The PEO@PIL exhibited a capacitance behaviour, which is improved with the presence of EMITFSI (PEO@PIL@IL). The capacitance is 3.7 F/g at a scan rate of 1 mV/s for PEO@PIL actuator and reaches 19.4 F/g in the case of PEO@PIL@IL actuator, thanks to the higher ionic conductivity that allows reducing the resistance and faster charging the CNT electrode surfaces.

Actuation performance of resulting dual-electrode actuator was then characterized using the coiled CNT yarn coated with PEO@PIL$^+$:TFSI$^-$, i.e. with mobile TFSI$^-$ anions, as the working electrode (WE) and the coiled CNT yarn coated with PEO@PIL:EMI$^+$, i.e. with mobile EMI$^+$ cations, as the counter-electrode (CE). Upon applying positive potential bias, the WE will be charged with anions and the CE with cations. Both electrodes are expected to undergo simultaneously the same degree of swelling, and thus produce the same expansion in coil diameter, and inducing a coordinated contraction of the dual-electrode actuator.

The tensile stroke of PEO@PIL actuator during a CV scan at 20 mV/s was measured from 3 V to −3 V. There is no obvious faradic reaction

observed for the dual-electrode in this range of potential (Fig. 4a) and the strain responses of dual-electrode actuators as a function of applied potential are shown in Fig. 4b and c. When the potential increase from 0 to 3 V, anions migrate to the working electrode with PIL^+:$TFSI^-$ based coating, while the cations move to the opposite one with PIL^-:EMI^+ based coating leading to the contraction of the yarn muscle, leading to a contraction, as expected. However, the maximum stroke of 0.05% was observed during the CV reverse scan from 3 V, indicating the stroke is delayed regarding the electrical stimulation (Fig. 4c). It might be caused by the relatively low ionic conductivity of the liquid-free PIL-based electrolyte inducing slow electrochemical charging and the not sufficient charging time. As expected from the presence of the polycationic and polyanionic coatings acting as selective ion blocking layers, the actuator presents a unipolar behaviour: the contraction is observed during positive bias and elongation during the reverse scan. Furthermore, the stroke variations were recorded under square potential waves between 3 to −3 V with different pulse times in order to reach full charge EDLC (Fig. 4d). The stroke increased up to 0.13% when the pulse time increased to 480 s.

Similar behaviour is observed with PEO@PIL@IL dual-electrode actuator. The tensile stroke during a CV scan at 20 mV/s was then measured and the PEO@PIL@IL dual-electrode actuator performances are presented in the Fig. 5a and b.

It was found that when the potential increased to 5 V, the contractile stroke reached 4%. The stroke kept increasing at the beginning of the reverse scan up to a maximum of 5.8% at 3 V, probably because of the still limited influx speed of ions to the rough coiled CNT surface. When pursuing the reverse potential scan further in the negative potentials (down to −3 V), only elongation of the actuator is observed, confirming that the unipolar behaviour is preserved in the presence of IL. The zero-charge potential appears to be shifted from 0 V to −3 V since bipolar deformation starts to be observed between −3 V and −4 V simultaneously with an obvious faradic reaction. Thus, optimal potential window was limited to −3 V and +5, it can also be extended to +6 V, allowed maximizing stroke while preserving the unipolar behaviour (Figure S3).

Due to the hysteresis of ion migration mentioned above, advanced cyclic voltammetry (CVA) scan, in which the potential is hold at 6 V for another 4 min after reaching the maximum vertex potential, was carried out to ensure that complete influx of ions to the CNT fully occurs before the reverse scan. As shown in the Fig. 6a and b, the contractile stroke increases from 4% to 10.5% when the potential is hold at 6 V for 4 min. Fig. 6c summarizes the schematic illustration of mechanism for the unipolar stroke of the dual-electrode actuator. When the positive potential is applied, anions from IL migrate to the working electrode, while the cations move to the opposite one leading to the contraction of the yarn muscle, as expected. When the potential changes to negative, the efflux of exogeneous and free-to-move counter-ions occurs from the coiled CNT yarns while influx of oppositely charged ions is blocked by the PIL coatings with same charge acting as ion selective layer. Consequently, only unipolar stroke is obtained in this range of potential (6 V to −3 V) even with the presence of free-to-move EMITFSI in the coating. When a lower negative potential of −4 V for instance is applied, the ion-repulsive effect of the selective PILs is overridden and a bipolar stroke is again observed. Finally, the hypothesis of the unipolar stroke caused by those two polycationic and polyanionic layers was definitely validated by the fabrication of another symmetric dual-electrolyte actuator made from coiled CNT coated similar but uncharged s-IPN ionogel where PILs are replaced by an uncharged polymer (C2000XL) resulting in PEO@C2000XL@IL. Such neutral coating promoted bipolar stroke deformation only (Figure S4).

The actuation of the PEO@PIL@IL dual-electrode actuator was also studied using consecutive square potential waves between 6 V to −3 V with different pulse times. Fig. 7a shows the stroke variation with pulse time. The actuator produces ~0.15% reversible linear contraction/expansion when 10 s positive/negative potential pulses were applied, with a slight baseline decline attributed to transitory stress relaxation under to chosen preload force. When the pulse time is increased, the

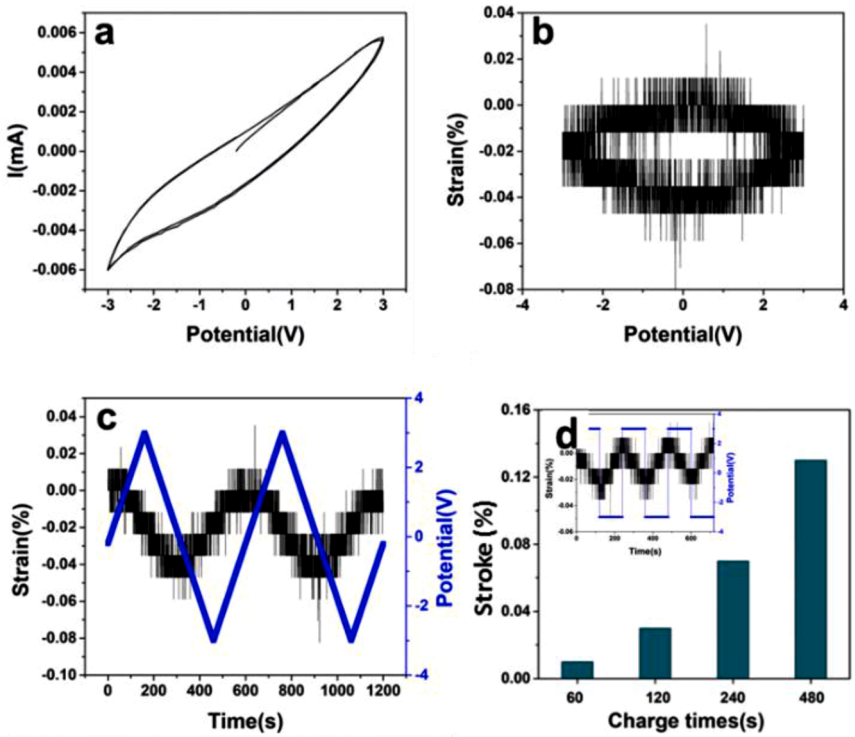

Fig. 4. (a) Cyclic voltammetry (CV) scans of the PEO@PIL dual-electrode actuator from 3 to −3 V at a scan rate of 20 mV/s. (b) Electrochemical tensile stroke measurements of the dual-electrode actuator at 25 mN preloading force with CV scan rate of 20 mV/s. (c) The tensile stoke variation of the dual-electrode actuator as a function of potential, (d) Tensile stroke as a function of charge time by using square potential wave stimulation (inset).

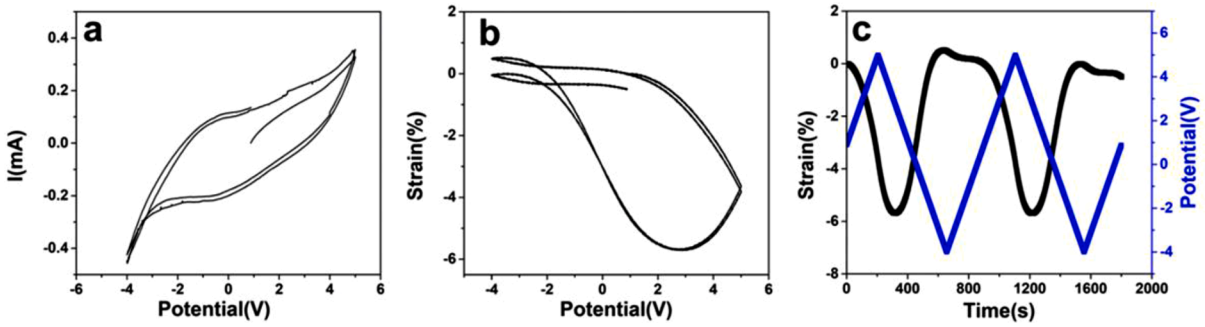

Fig. 5. (a) CV scans curves of PEO@PIL@IL actuator at a scan rate of 20 mV/s. (b) Electrochemical tensile stroke measurements of the PEO@PIL@IL actuator at 25 mN extra force with the CV scan rate of 20 mV/s. (c) The tensile stoke of the dual-electrolyte actuator contained EMITFSI as a function of potential.

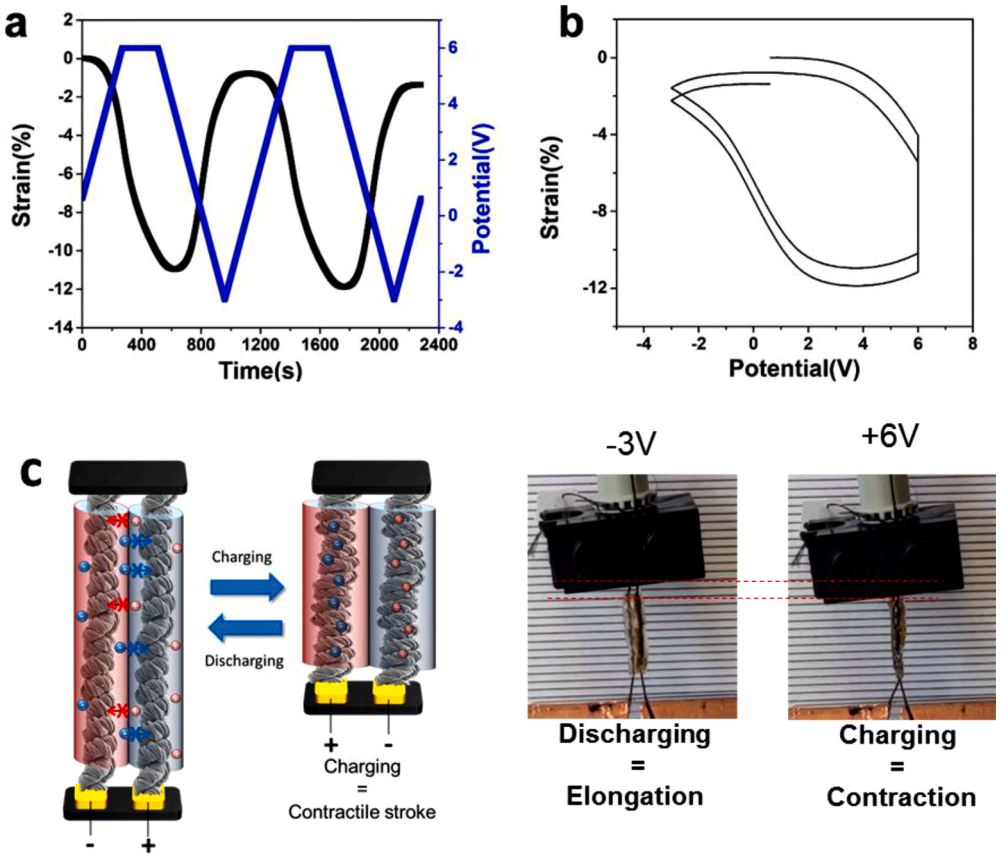

Fig. 6. (a) Electrochemical tensile stroke measurements of dual-electrolyte actuator containing EMITFSI with 25 mN preload force for cyclic voltammetry advanced (CVA) cycles. The potential is scan between −3 V and 6 V at a scan rate of 20 mv/s, and then the potential is kept at 6 V for 4 min to ensure the stroke up to the maximum. (b) The electrochemical tensile stroke variation at different potentials. (c) Schematic of the mechanism of electrochemical tensile stroke of dual-electrolyte actuator containing EMITFSI with captions of the contractile response.

actuator's stroke exhibits a rapid increase, as shown in Fig. 7b. With a pulse time of 480 s (figure S5), the actuator presents a large stroke of 9.5% comparable with the literature of air-operating CNT yarn actuators (Table S1). Meanwhile, the energy density of the actuator was calculated by measuring the actuation displacement under different preloads (Fig. 7c and Figure S6), which shows a maximum value of 20 J/kg (work capacity of 3.10^{-5} Nm). Interestingly, the values are perfectly located in the range of nature muscles' energy density (0.4–40 J/kg) [34]. The stability of the open-air actuation of the CNT yarn actuator upon cycling was also investigated. The measured stroke over 80 cycles is shown in Fig. 7d, remaining almost constant, around 9–10%, and confirming the stability of these capacitive CNT yarn actuators in open-air. The initial baseline decline is here also observed during first cycles before stabilizing upon longer cycling. Fluctuations in the baseline of Fig. 7d at longer times can be attributed to the variation in ambient temperature between night and day.

3.4. Strategies to enhance the actuation performance of dual-electrode actuator

The fast response of an actuator is an important feature for selecting the desired applications. Here, the actuator's response speed is governed by both the ionic conductivity of the ionic conducting layers and by the bulk resistance which depends to distance between electrodes. So, a thinner dual-electrode actuator in which the interval distance between the two coiled yarns is decreased from 1 mm to 0.45 mm was fabricated (Fig. 8a and Figure S7). The stroke variation with different pulse times in the square potential waves changing from 6 to −3 V were recorded, and the measured stroke reached up to ~9.7% at 240 s pulse time (Fig. 8b). That is, the response time is halved compared with the previous actuator with a 1 mm gap. This result is consistent with the proportional reduction of distance between electrodes (Fig. 8c). It is worthy to note that the dual-electrode actuator exhibits a contractile stroke accompanied with twisting (Fig. 8d and Video S1). Such twisting behaviour could be caused

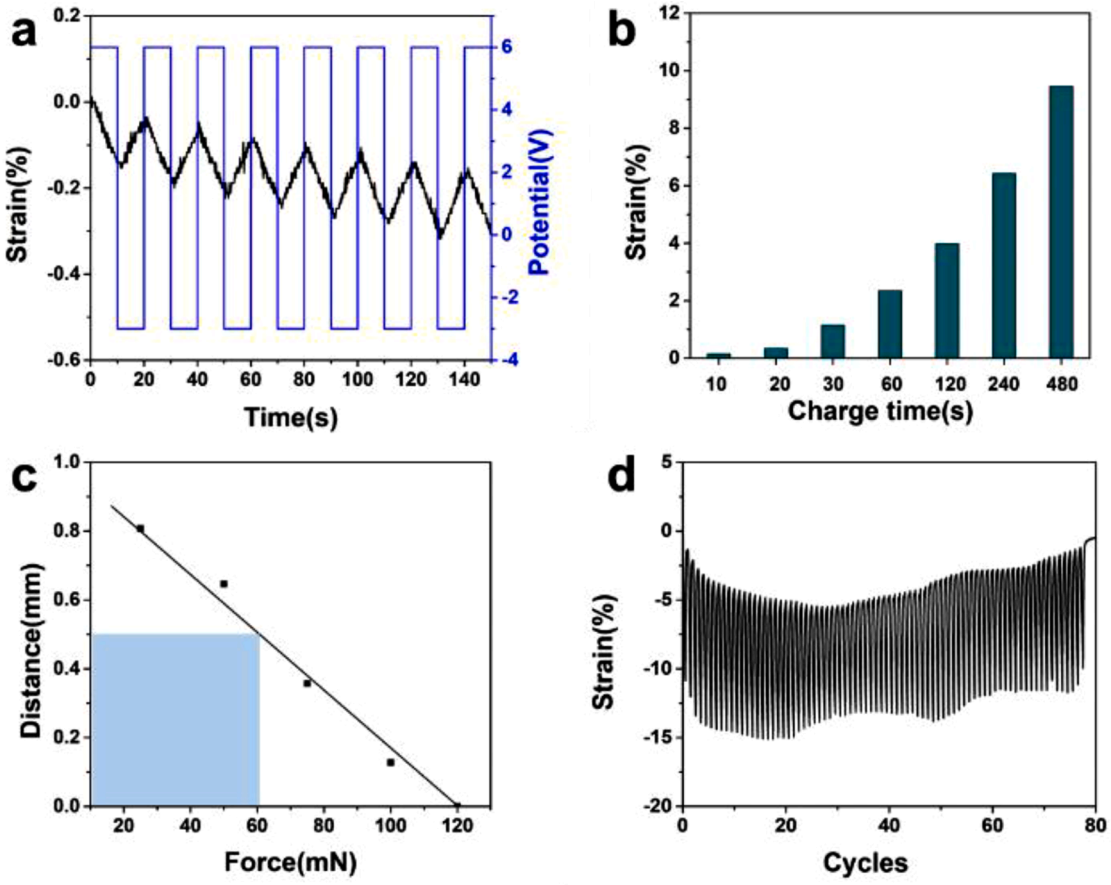

Fig. 7. (a) Electrochemical tensile stroke measurements of the PEO@PIL@IL dual-electrode actuator at 25 mN preload force for chronoamperometry cycles. The square potential waves changed from 6 to −3 V with 10s-pulse time. (b) The stroke variation of the dual-electrode actuator with different pulse times. (c) The energy density of the dual-electrode actuator. The corresponding displacements are measured with different preloads. (d) The stroke stability upon cycling of dual-electrode actuator in open-air condition was realized by using a square potential wave changed from 6 to −3 V with 480 s pulse.

by the unfastening process of the coiled CNT during the electrochemical stimulation. The ions migrate to the coiled CNT upon charging, resulting in the contraction behaviour. At the same time, the swollen and coiled CNT yarns exhibit a slight overcoiling process which is partially inhibited by the coated ionogel sheaths. Thus, this dual-electrode coiled CNT actuator exhibits a visible tortional motion at low preload which can be effectively reduced upon increasing the preload force to finally achieve a straighter contractile deformation. As a demonstration, when the preloading force is 5-fold higher (from 25 to 125 mN), the stroke slightly decreases from 9.7 to 8% (Figure S8), while the twisting behaviour of the actuator almost disappears (Video S2).

Finally, to further enhance the responsiveness and usefulness of dual-electrode actuator, a higher potential bias between −6 V and 9 V has been applied to the actuator but with shorter pulse time. To check first if the coiled CNT muscle was stable in these conditions, a CV scan with 500 mV/s scan rate was performed (Figure S9a). No Faradic reaction is observed in this potential window at such high scan rate, indicating that applying high potential for short time preserves the electrochemical stability. Then, a consecutive square wave potential stimulation between −6 V to 9 V with 2 s pulses was carried out, leading to a ~0.2% displacement of the actuator (Figure S9b). The electrochemical cycling performance of the actuator shows that it maintained a stable strain of 0.15% over 2000 cycles in these conditions (Figure S9c).

4. Conclusions

An air-stable dual-electrode yarn actuator composed of coiled CNT yarns coated with two ionogels designed on purpose, i.e. polycationic and polyanionic ionogels, has been developed. The two polyionic coatings are developed as semi-interpenetrating polymer networks, combining a photocured PEO network, an entangled cationic or anionic linear polymeric ionic liquid and additional ionic liquid. These materials present low initial viscosity and fast curing making them suitable for electroactive yarn coating applications.

The solid-state dual-electrode actuator exhibits a unipolar contractile stroke up to 9.7% upon electrochemical stimulation in open air. The unipolar behaviour of the actuator is provided by a cationic-anionic junction, similar to the p-n junction of semiconductors, that can block the movement of the ions during the reversal of the potential. The blocking effect is caused by the repulsion effect between ions of the same charge as those grafted onto entangled polymeric ionic liquid backbone. Thanks to the stable nature of both PIL and ionic liquid, long operational lifetime in the open air was achieved with no loss of performances after 2000 cycles.

The dual-electrode yarn actuator's response speed remains slow due to the ion-diffusion limited process but was improved by either decreasing the gap between the two electrodes or applying higher potential with short pulse times.

The development of such air-stable linear yarn actuators based on commercially available CNT yarns makes it widely accessible for mechanical engineering and opens a horizon for their integration in soft robotics. Furthermore, these thin yarn devices allow using weaving or inlay knitting to act as textile actuators in applications such as haptic garments, wearable robotics and soft, textile exoskeletons.

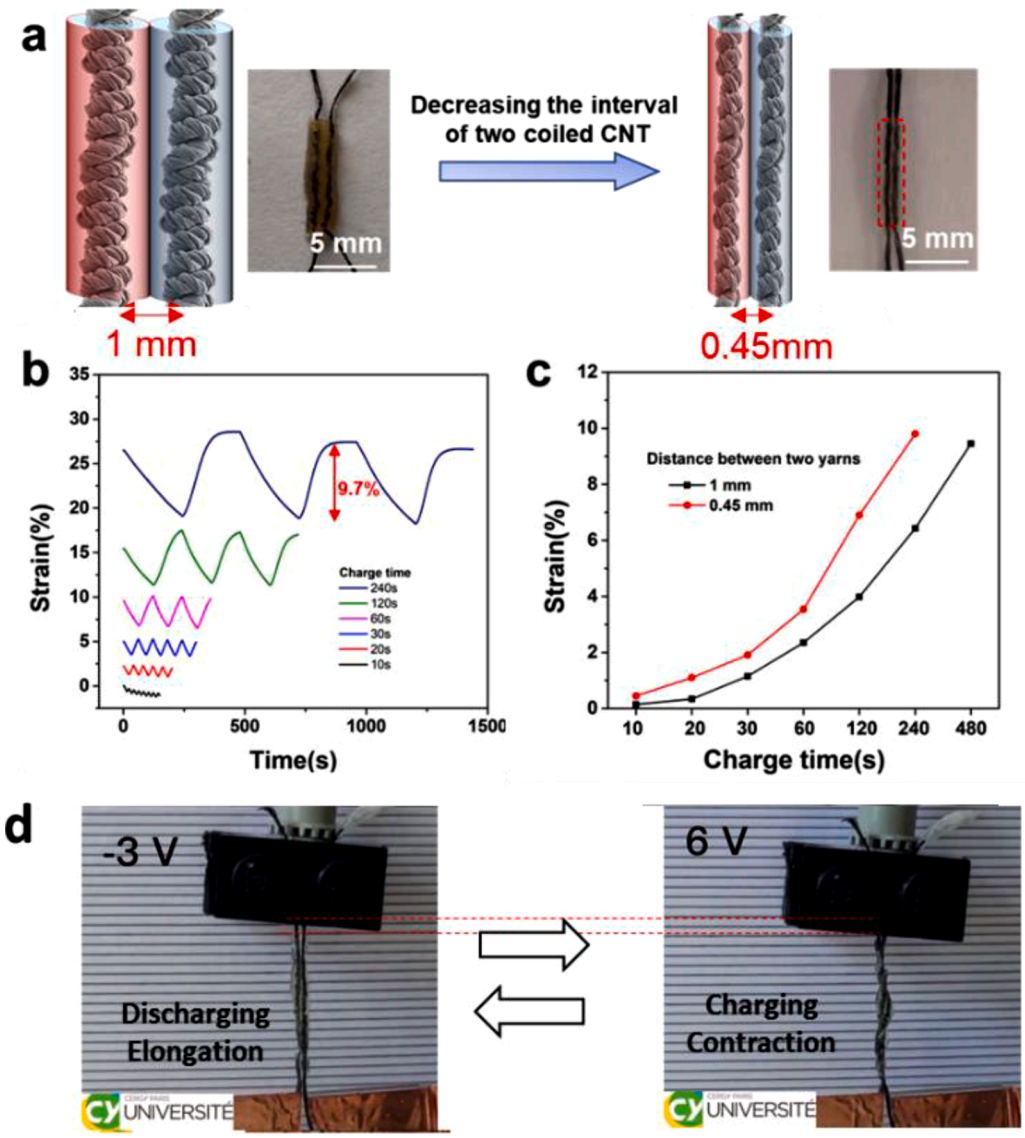

Fig. 8. (a) The schematic illustration and images of dual electrodes actuators containing EMITFSI with different distances between two electrolytes. (b) The stroke curves of dual-electrode actuator with a 0.45 mm gap between the two electrodes as a function of pulse times. (c) The data comparison of stroke from dual-electrolyte actuators with different gap between the two electrodes. (d) dual-electrode actuators on their elongation and contraction state, demonstrating the twising behaviour.

CRediT authorship contribution statement

Bin Ni: Investigation, Methodology, Writing – original draft. **Frédéric Braz Ribeiro:** Investigation, Methodology. **Cédric Vancaeyzeele:** Conceptualization, Validation, Writing – review & editing. **Giao T.M. Nguyen:** Conceptualization, Validation, Writing – review & editing. **Edwin W.H. Jager:** Writing – review & editing, Funding acquisition. **Frédéric Vidal:** Conceptualization, Validation, Writing – review & editing. **Cédric Plesse:** Conceptualization, Validation, Resources, Supervision, Funding acquisition, Project administration.

Declaration of Competing Interest

The authors declare that they have no known competing financial interests or personal relationships that could have appeared to influence the work reported in this paper.

Data availability

Data will be made available on request.

Acknowledgments

The authors would like to thank the European Union's Horizon 2020 research and innovation program under grant agreement no. 825232 "WEAFING." The author would like to thank the Conseil regional île de France for funding the Cerasem project (grant:15013107) that has allowed the acquisition of a ZEISS Gemini SEM 300.

Supplementary materials

Supplementary material associated with this article can be found, in the online version, at doi:10.1016/j.apmt.2023.101756.

References

[1] S.M. Mirvakili, D. Sim, I.W. Hunter, R. Langer, Actuation of untethered pneumatic artificial muscles and soft robots using magnetically induced liquid-to-gas phase transitions, Sci. Robot. 5 (2020) eaaz4239, https://doi.org/10.1126/scirobotics.aaz4239.

[2] H.M. Herr, R.D. Kornbluh, New horizons for orthotic and prosthetic technology: artificial muscle for ambulation. Proc.SPIE, 2004, https://doi.org/10.1117/12.544510.

[3] C. Lescano, C. Herrera, R. Mirabal, R. Rodrigo, S. Rodrigo, Characterization of a pneumatic artificial muscle for its application in an active ankle-foot orthosis, J. Phys. Conf. Ser. (2013) 477, https://doi.org/10.1088/1742-6596/477/1/012040.
[4] B. Ni, G. Liu, M. Zhang, M. Tatoulian, P. Keller, M.-.H. Li, Customizable sophisticated three-dimensional shape changes of large-size liquid crystal elastomer actuators, ACS Appl. Mater. Interfaces. 13 (2021) 54439–54446, https://doi.org/10.1021/acsami.1c18424.
[5] C.S. Haines, M.D. Lima, N. Li, G.M. Spinks, J. Foroughi, J.D.W. Madden, S.H. Kim, S. Fang, M. Jung de Andrade, F. Göktepe, Ö. Göktepe, S.M. Mirvakili, S. Naficy, X. Lepró, J. Oh, M.E. Kozlov, S.J. Kim, X. Xu, B.J. Swedlove, G.G. Wallace, R. H. Baughman, Artificial muscles from fishing line and sewing thread, Science 343 (80) (2014) 868–872, https://doi.org/10.1126/science.1246906.
[6] E.W. Hawkes, L.H. Blumenschein, J.D. Greer, A.M. Okamura, A soft robot that navigates its environment through growth, Sci. Robot. 2 (2017) eaan3028, https://doi.org/10.1126/scirobotics.aan3028.
[7] K. Hosoda, Y. Sakaguchi, H. Takayama, T. Takuma, Pneumatic-driven jumping robot with anthropomorphic muscular skeleton structure, Auton. Robots. 28 (2010) 307–316, https://doi.org/10.1007/s10514-009-9171-6.
[8] Y. Wang, J. Qiao, K. Wu, W. Yang, M. Ren, L. Dong, Y. Zhou, Y. Wu, X. Wang, Z. Yong, J. Di, Q. Li, High-twist-pervaded electrochemical yarn muscles with ultralarge and fast contractile actuations, Mater. Horizons. 7 (2020) 3043–3050, https://doi.org/10.1039/D0MH01352H.
[9] S. Aziz, J.G. Martinez, B. Salahuddin, N.-.K. Persson, E.W.H. Jager, Fast and High-Strain Electrochemically Driven Yarn Actuators in Twisted and Coiled Configurations, Adv. Funct. Mater 31 (2021), 2008959, https://doi.org/10.1002/adfm.202008959.
[10] J.S. Hyeon, J.W. Park, R.H. Baughman, S.J. Kim, Electrochemical graphene/carbon nanotube yarn artificial muscles, Sensors Actuators B Chem 286 (2019) 237–242, https://doi.org/10.1016/j.snb.2019.01.140.
[11] H. Chu, X. Hu, Z. Wang, J. Mu, N. Li, X. Zhou, S. Fang, C.S. Haines, J.W. Park, S. Qin, N. Yuan, J. Xu, S. Tawfick, H. Kim, P. Conlin, M. Cho, K. Cho, J. Oh, S. Nielsen, K.A. Alberto, J.M. Razal, J. Foroughi, G.M. Spinks, S.J. Kim, J. Ding, J. Leng, R.H. Baughman, Unipolar stroke, electroosmotic pump carbon nanotube yarn muscles, Science 371 (80–) (2021) 494–498, https://doi.org/10.1126/science.abc4538.
[12] J.A. Lee, N. Li, C.S. Haines, K.J. Kim, X. Lepró, R. Ovalle-Robles, S.J. Kim, R. H. Baughman, Electrochemically powered, energy-conserving carbon nanotube artificial muscles, Adv. Mater. 29 (2017), 1700870, https://doi.org/10.1002/adma.201700870.
[13] J. Qiao, J. Di, S. Zhou, K. Jin, S. Zeng, N. Li, S. Fang, Y. Song, M. Li, R. H. Baughman, Q. Li, Large-stroke electrochemical carbon nanotube/graphene hybrid yarn muscles, Small 14 (2018), 1801883, https://doi.org/10.1002/smll.201801883.
[14] R.H. Baughman, C. Cui, A.A. Zakhidov, Z. Iqbal, J.N. Barisci, G.M. Spinks, G. G. Wallace, A. Mazzoldi, D. De Rossi, A.G. Rinzler, O. Jaschinski, S. Roth, M. Kertesz, Carbon nanotube actuators, Science 284 (80) (1999) 1340–1344, https://doi.org/10.1126/science.284.5418.1340.
[15] A. Maziz, C. Plesse, C. Soyer, C. Chevrot, D. Teyssié, E. Cattan, F. Vidal, Demonstrating kHz frequency actuation for conducting polymer microactuators, Adv. Funct. Mater. 24 (2014) 4851–4859, https://doi.org/10.1002/adfm.201400373.
[16] X. Liu, B. He, Z. Wang, H. Tang, T. Su, Q. Wang, Tough nanocomposite ionogel-based actuator exhibits robust performance, Sci. Rep. 4 (2014) 6673, https://doi.org/10.1038/srep06673.
[17] M. Ren, J. Qiao, Y. Wang, K. Wu, L. Dong, X. Shen, H. Zhang, W. Yang, Y. Wu, Z. Yong, W. Chen, Y. Zhang, J. Di, Q. Li, Strong and robust electrochemical artificial muscles by ionic-liquid-in-nanofiber-sheathed carbon nanotube yarns, Small 17 (2021), 2006181, https://doi.org/10.1002/smll.202006181.
[18] C. Feng, C.P. Hemantha Rajapaksha, A. Jákli, Ionic elastomers for electric actuators and sensors, Engineering 7 (2021) 581–602, https://doi.org/10.1016/j.eng.2021.02.014.
[19] J.Le Bideau, L. Viau, A. Vioux, Ionogels, ionic liquid based hybrid materials, Chem. Soc. Rev. 40 (2011) 907–925, https://doi.org/10.1039/c0cs00059k.
[20] Y. Zhong, G.T.M. Nguyen, C. Plesse, F. Vidal, E.W.H. Jager, Highly conductive, photolithographically patternable ionogels for flexible and stretchable electrochemical devices, ACS Appl. Mater. Interfaces 10 (2018) 21601–21611, https://doi.org/10.1021/acsami.8b03537.
[21] Y. Ding, J. Zhang, L. Chang, X. Zhang, H. Liu, L. Jiang, Preparation of high-performance ionogels with excellent transparency, good mechanical strength, and high conductivity, Adv. Mater. 29 (2017), 1704253, https://doi.org/10.1002/adma.201704253.
[22] B. Yiming, Y. Han, Z. Han, X. Zhang, Y. Li, W. Lian, M. Zhang, J. Yin, T. Sun, Z. Wu, T. Li, J. Fu, Z. Jia, S. Qu, A mechanically robust and versatile liquid-free ionic conductive elastomer, Adv. Mater. 33 (2021), 2006111, https://doi.org/10.1002/adma.202006111.
[23] H.J. Kim, B. Chen, Z. Suo, R.C. Hayward, Ionoelastomer junctions between polymer networks of fixed anions and cations, Science 367 (80) (2020) 773–776, https://doi.org/10.1126/science.aay8467.
[24] A. Maziz, A. Concas, A. Khaldi, J. Stålhand, N.-.K. Persson, E.W.H. Jager, Knitting and weaving artificial muscles, Sci. Adv. 3 (2022), e1600327, https://doi.org/10.1126/sciadv.1600327.
[25] N.-.K. Persson, J.G. Martinez, Y. Zhong, A. Maziz, E.W.H. Jager, Actuating Textiles: next Generation of Smart Textiles, Adv. Mater. Technol. 3 (2018), 1700397, https://doi.org/10.1002/admt.201700397.
[26] J. Abel, J. Luntz, D. Brei, Hierarchical architecture of active knits, Smart Mater. Struct. 22 (2013), 125001, https://doi.org/10.1088/0964-1726/22/12/125001.
[27] R. Granberry, K. Eschen, B. Holschuh, J. Abel, Functionally graded knitted actuators with NiTi-based shape memory alloys for topographically self-fitting wearables, Adv. Mater. Technol. 4 (2019), 1900548, https://doi.org/10.1002/admt.201900548.
[28] R. Temmer, A. Maziz, C. Plesse, A. Aabloo, F. Vidal, T. Tamm, search of better electroactive polymer actuator materials: pPy versus PEDOT versus PEDOT–PPy composites, Smart Mater. Struct. 22 (2013), 104006, https://doi.org/10.1088/0964-1726/22/10/104006.
[29] H.-.N. Kwon, S.-.J. Jang, Y.C. Kang, K.C. Roh, The effect of ILs as co-salts in electrolytes for high voltage supercapacitors, Sci. Rep. 9 (2019) 1180, https://doi.org/10.1038/s41598-018-37322-y.
[30] P. Bonhôte, A.-.P. Dias, N. Papageorgiou, K. Kalyanasundaram, M. Grätzel, Hydrophobic, highly conductive ambient-temperature molten salts †, Inorg. Chem. 35 (1996) 1168–1178, https://doi.org/10.1021/ic951325x.
[31] D.O. Ponkratov, E.I. Lozinskaya, P.S. Vlasov, P.-.H. Aubert, C. Plesse, F. Vidal, Y. S. Vygodskii, A.S. Shaplov, Synthesis of novel families of conductive cationic poly (ionic liquid)s and their application in all-polymer flexible pseudo-supercapacitors, Electrochim. Acta. 281 (2018) 777–788, https://doi.org/10.1016/j.electacta.2018.05.191.
[32] M.D. Lima, N. Li, M. Jung de Andrade, S. Fang, J. Oh, G.M. Spinks, M.E. Kozlov, C. S. Haines, D. Suh, J. Foroughi, S.J. Kim, Y. Chen, T. Ware, M.K. Shin, L. D. Machado, A.F. Fonseca, J.D.W. Madden, W.E. Voit, D.S. Galvão, R. H. Baughman, Electrically, Chemically, and Photonically Powered Torsional and Tensile Actuation of Hybrid Carbon Nanotube Yarn Muscles, Science 338 (80–) (2012) 928–932, https://doi.org/10.1126/science.1226762.
[33] Y. Zhong, G.T.M. Nguyen, C. Plesse, F. Vidal, E.W.H. Jager, Tailorable, 3D structured and micro-patternable ionogels for flexible and stretchable electrochemical devices, J. Mater. Chem. C. 7 (2019) 256–266, https://doi.org/10.1039/C8TC04368J.
[34] M. Duduta, E. Hajiesmaili, H. Zhao, R.J. Wood, D.R. Clarke, Realizing the potential of dielectric elastomer artificial muscles, Proc. Natl. Acad. Sci. 116 (2019) 2476–2481, https://doi.org/10.1073/pnas.1815053116.